PCCP

ROYAL SOCIETY OF CHEMISTRY

PAPER

Cite this: *Phys. Chem. Chem. Phys.*, 2024, **26**, 17854

Electronic correlations and intrinsic magnetism of interstitial quasi-atomic states in Li_8Au electride†

Dmitry Y. Novoselov, *[abc] Dmitry M. Korotin, [ab] Alexey O. Shorikov, [abc] Vladimir I. Anisimov [abc] and Artem R. Oganov [c]

We investigate the electronic sub-system of a recently designed Li_8Au superconducting electride to reveal its many-body correlated nature and magnetic properties. Using maximally localized Wannier functions (MLWFs) to describe the interstitial anion electron (IAE) states, it was found that these states are partially occupied with a population of $1.5e^-$ and have negligible hybridization with the almost completely filled p-Au states. The averaged interaction screened Hubbard parameter U for quasi-atomic IAE states evaluated by the constrained random-phase approximation (CRPA) method is 2 eV, comparable to the width of the electride band suggesting moderate electronic correlations. Using dynamical mean field theory (DMFT) approach we found that IAEs in Li_8Au electride behave as magnetic centers and possess their own well localised magnetic moments of $0.5\mu_B$ per quasi-atomic IAE. The obtained results deepen the understanding of the significance of many-body effects in the IAE subsystem of electronic states and reveal the mechanism for the formation of intrinsic magnetic moments on IAEs, which behave like ferromagnetic quasi-atoms in the Li_8Au electride. Overall, the observed correlation effects in Li_8Au emphasize their importance in materials with excess electrons confined in cavities.

Received 12th April 2024,
Accepted 1st June 2024

DOI: 10.1039/d4cp01508h

rsc.li/pccp

1 Introduction

Electrides are an unusual class of materials where interstitial anionic electrons (IAEs) are trapped in ordered cavities of a positively charged lattice framework. In contrast to conventional ionic crystals, in electrides the set of occupied energy bands cannot be decomposed as a sum of band representations (BRs) induced by only atomic orbitals in crystals, but necessarily should includes BRs of quasi-atomic orbitals centered at electride sites.[1] The wave functions of such electrons confined in anion vacancy positions exhibit a unique duality, combining strong localization and spatial extent caused by the competition between the kinetic energy and Coulomb interactions. Such rivalry leads to the realization of a complex many-body ground state. In some cases, the coupling between subsystems of atomic and interstitial electrons is so weak that the latter can be considered separately, thereby creating a remarkable platform for the implementation and study of phenomena in pure quantum electronic systems.[2,3] In particular, such treatment led to the discovery of the Wigner-crystal[4] state on the electride surface.[5] Besides, peculiarities of electride states lead to several intriguing properties such as high carrier concentration,[6] low work function[7] and high electron mobility[6] as well as surface magnetism.[8] These properties offer electrides wide prospects for applications[9] in spintronics, electron emission devices,[10] high-performance catalysis,[11,12] rechargeable ion batteries,[13] superconductivity.[14,15]

As shown earlier, predictions based on density functional theory (DFT) level are not always able to fully reflect the physics of the electride subsystem since many-body effects need to be taken into account.[16–24] Usually, electron correlation effects enrich the physics of the phenomena that occur in materials and dramatically improve their functionality, and electrides are not an exception to this rule. It has been recently discovered that some electrides may possess a specific type of intrinsic magnetism unrelated to the electronic subsystem of atoms.[19,25–32] However, understanding the relevance of many-body effects in the subsystem of electronic interstitial states, as well as the mechanisms of formation of their intrinsic magnetic moments in various electrides, remains to be elucidated.

This study focuses on the investigation of Li_8Au, a recently predicted dynamically stable electride[33] with the highest critical temperature of the transition to the superconducting state T_c of 73.1 K at 250 GPa revealed to date among electrides. This system resembles both high-T_c hydrides[34] and Na_2He electride,[35] with high-symmetry building blocks. Since the assumed space of IAE localization in Li_8Au is quite restricted and the

[a] *M.N. Mikheev Institute of Metal Physics of the Ural Branch of the Russian Academy of Sciences, 18 S. Kovalevskaya St., Yekaterinburg, 620108, Russia. E-mail: novoselov@imp.uran.ru*
[b] *Skolkovo Institute of Science and Technology, 30 Bolshoy Boulevard, bld. 1, Moscow, 121205, Russia*
[c] *Department of Theoretical Physics and Applied Mathematics, Ural Federal University, 19 Mira St., Yekaterinburg 620002, Russia*

† Electronic supplementary information (ESI) available. See DOI: https://doi.org/10.1039/d4cp01508h

interstitial electronic states are described by a partially filled rather narrow energy band, one should examine this system with respect to the possible appearance of electronic correlation effects and inherent magnetism in the IAE subsystem.

2 Results and discussion

Well-localized interstitial anionic electrons in the cavities of electrides can be generalized and considered as interstitial quasi-atoms (ISQs), where IAEs occupy quantized orbitals of interstitial sites.[36] The Li_8Au structure represents a double *fcc* lattice possessing the $Fm\bar{3}m$ space group[32] with atomic Au and positively charged cubic Li_8 cages accommodating ISQs. Calculations of the phonon spectrum have shown that this structure is dynamically stable over a wide pressure range from 120 to 300 GPa.[32] Fig. 1(a) shows the isosurfaces of the electron localization function (ELF)[37] obtained from the DFT charge density where it is clearly seen that the charge density is confined at the center of the lithium cubes (4*a* Wyckoff positions) and is well localized with ELF = 0.9. The absence of any contribution on Au atoms suggests that the electron localization on the valence p-Au shell is weaker than that for IAEs.

Following the ELF shape and the idea of ISQs, we consider Li_8Au as a crystal with the rocksalt-type lattice formed by ISQs ions at 4*a* Wyckoff position and Au ions at 4*b* Wyckoff position. Consequently, our goal is to map the band structure obtained within DFT to the basis of wave functions centered on the nodes of this new lattice.

To describe properly the wave functions of spatially localized electrons located at the anion sites we construct the maximally localized Wannier functions.[38] The trial wave function of *s*-symmetry was initiated at the ISQ Wyckoff positions. After the disentanglement and localization process, the MLWF changed its shape to reflect the local symmetry of the electride state. The basis set also contained three Wannier functions with the symmetry of Au p-states. For the MLWFs construction we used the energy window spanned by energy bands in the range from −2.5 to 1.5 eV relative to the Fermi level. Besides the electride states, this energy interval also contains p-Au energy bands. Fig. 1(b) shows the spatial distribution of the resulting wave functions describing the ISQ and p-Au states.

The ISQ state's initial *s*-symmetry is generally preserved during the disentanglement and maximally localization procedures. The only difference is that it has extended tails along the main diagonals of the cube (not shown in Fig. 1) connecting neighboring electride sites to each other. The presence of these overlapping regions of the electride wave-functions provides interstitial electrons the possibility to hop between neighboring cavities, and also forms a channel for direct exchange interactions.

The Li_8Au band structure shown in Fig. 2 contains three peculiar points along the directions Γ–X, K–Γ and Γ–L (marked by dashed circles), corresponding to the orientations towards the nearest Au atoms in real space which are 2.85 Å away from ISQ. The Au and ISQ energy bands undergo a discontinuity associated with the formation of a gap between −1.5 and −0.8 eV at these points. The appearance of extrema and the opening of a gap in the band structure between high-symmetry points along the Γ–X, K–Γ and Γ–L directions indicate a symmetry breaking of the wave vectors.[39] The p-Au triply degenerate band at the Γ point has T_{1u} symmetry, while the underlying band corresponding to the s-ISQ has A_{1g} symmetry. At the high-symmetry point X, a splitting of the p-Au state into a doubly degenerate with E_u symmetry and an underlying A_{2u} state is observed, with the s-ISQ band with A_{1g} symmetry on top. Thus, the symmetry of the lowest energy band undergoes a change at the path along the high symmetry Γ–X direction. This break leads to restrictions on the electron transfer between the electride subsystem and the subsystem of atomic electronic states, as they need to overcome the energy barrier determined by the value of the corresponding energy gap. The presence of local extrema in the band structure highlights the origin of Van Hove singularities, which were mentioned in paper.[33] Except for these three special points, the energy bands of the two electron subsystems p-Au and ISQ reveal no coupling in the rest of the Brillouin zone. The hopping parameter t_{sp} between the ISQ and p-Au states is only 0.02 eV. Thus, two spatially separated weakly coupled electronic subsystems with completely independent contributions to the density of states at the Fermi level coexist in Li_8Au in the same energy range.

Fig. 2 shows that the Fermi level is crossed by the energy bands of both ISQ and triply degenerate p-Au states. This

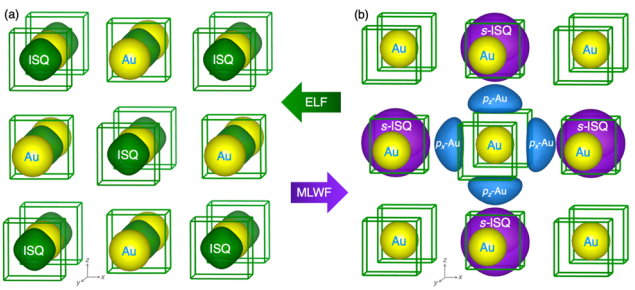

Fig. 1 Crystal structure of Li_8Au with isosurfaces of ELF = 0.9 in green (a) and some isosurfaces of the square of MLWFs of ISQs in violet as well as MLWFs of p_z, p_x-Au in cyan (b). Yellow spheres correspond to Au atoms, while Li atoms are located in the vertices of the green-lined cubes.

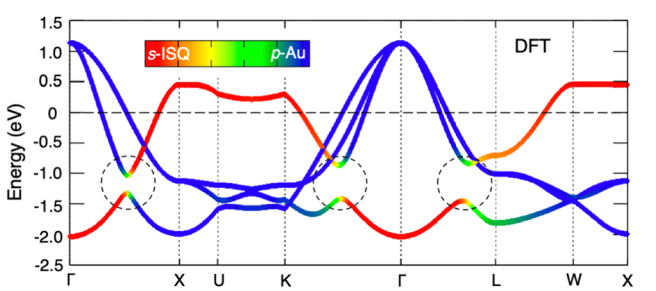

Fig. 2 MLWFs projected energy bands of Li_8Au obtained from DFT calculation. The color scale encodes the weight balance between the contribution of interstitial and p-Au states to the energy bands. The special points are marked with dashed circles.

indicates that the Fermi surface of Li_8Au is formed by sheets of both electronic subsystems. Therefore, the electronic conductivity of this material should have contributions from interstitial electrons as well as from electrons assigned to Au atoms.

The formation of bonds in Li_8Au is followed by charge transfer, where eight lithium atoms donate one electron each from their partially filled 2s shells. These 8 electrons are redistributed as follows, $1.5e^-$ go to form the IAE state, and another $6.5e^-$ are accepted by the Au atom ($1e^-$ for 6s and $5.5e^-$ for 6p). Integrating the density of states of the IAE described by MLWF up to the Fermi level indeed gives the number of electrons in the Li_8-cavity equal to $1.5e^-$.

As shown in Fig. 2, the ISQ energy band contains two rather flat regions along the *X*–*U*–*K* and *W*–*X* directions of the first Brillouin zone, which along with the relatively small width of this band ($\sim$2.5 eV), its partial filling, and strong spatial localization allow one to expect the presence of essential electronic correlations in this subsystem.

To evaluate the role of Coulomb correlation effects in the formation of the electronic structure of Li_8Au electride, we calculated the value of the averaged screened interaction Hubbard parameter U for ISQ electronic states using constrained random-phase approximation (cRPA) method.[40,41] We have evaluated Coulomb matrix elements U_{ijkl} (ω = 0) and obtained a Hubbard U parameter equal to 2.024 eV. This value is consistent with the values that are typical for other electrides with well-localized IAEs states.[16–21,24] The obtained magnitude of the U parameter is comparable to the width of the ISQ energy band, supporting the presence of essential correlation effects in the interstitial electronic sub-system of Li_8Au. At the same time, since p-Au states are triply degenerate, more extended in space than s-ISQ, and almost completely occupied, one should not expect substantial correlation effects on them.

At the next stage, using the obtained basis of MLWFs including functions describing ISQ and p-Au states, a small non-interacting Hamiltonian was constructed. To account for many-body effects in the electride subsystem, this Hamiltonian was then solved using the DMFT[42] technique with U = 2 eV and with allowance for spin polarization.

Based on DMFT calculations at β = 30 eV^{-1}, the *k*-resolved spectral functions $A(k, \omega)$ were obtained and are shown in Fig. 3 for two spin projections and could be directly compared with angle-resolved photoemission spectroscopy (ARPES). As can be seen from this figure, the initially degenerate ISQ band has split into two bands. At the same time, the bands corresponding to the p-Au states remained the same as they were at the DFT level. It is also worth noting that no spin polarization was obtained in the DFT calculation. Fig. 4 shows spin-resolved density of states evaluated by an analytical continuation of a self-energy dependence from Matsubara to the real frequencies using the Padé approximation method.[43] It follows from both figures that the electride valence band is spin-polarized and for spin-up orientation it is completely filled while for spin-down orientation it is partially filled. Thus, the Li_8Au electride subsystem reveals a typical half-metallic character and, like all half-metals, should be ferromagnetic. The IAE wave functions tails' overlap creates a path of direct ferromagnetic exchange interaction with the first nearest neighbors. To ensure that we do not overlook essential physics related to magnetic properties and behavior near the Fermi level by neglecting correlation effects on the p-Au states, we performed calculations using the HSE hybrid functional.[44] The occurrence of local magnetic moments on the interstitial electronic states, as well as the energy dispersion, were found to be qualitatively reproduced by the hybrid functional in agreement with the results of our DMFT calculation (see ESI†). This confirms that electronic correlation effects are significant solely for s-ISQ states, thereby justifying the application of a minimal basis set in DMFT calculations.

The substantial magnetic moment of spin-polarized IAE states up to 0.5 μ_B indicates that they behave as magnetic elements in a nonmagnetic lattice framework. The dual nature due to the localization and extent of the spatial distribution of the anionic electronic states can cause the existence of unique magnetic mechanisms in intrinsic magnetic electrides,[26] which deserve further research.

To investigate magnetic properties, we calculated spin–spin correlation functions on the imaginary time axis $\langle S_z(\tau)S_z(0)\rangle$ and in the frequency domain $\langle S_z(\omega)S_z(0)\rangle$ in a wide temperature

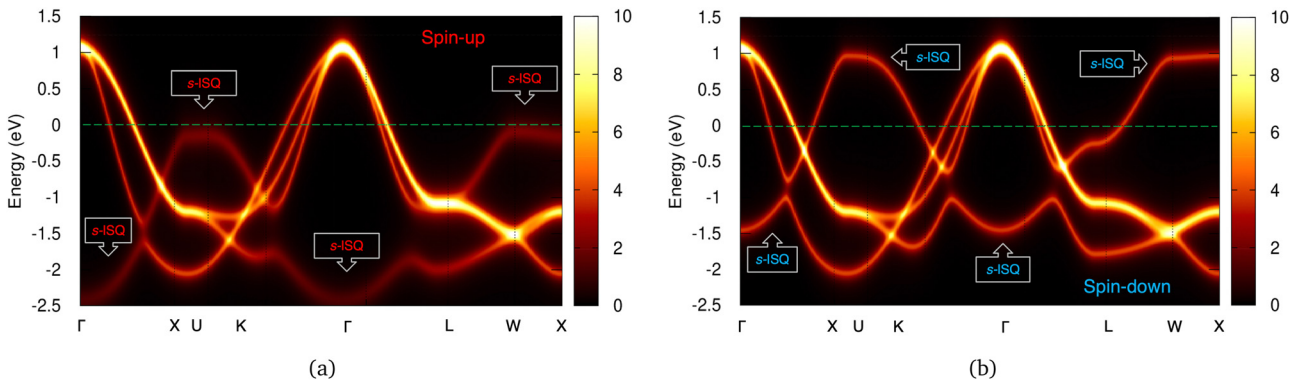

Fig. 3 *k*-Resolved total spectral functions $A(k, \omega)$ of Li_8Au obtained by DMFT calculation at β = 30 eV^{-1} for spin-up (a) and spin-down (b). The green dashed line shows the Fermi level.

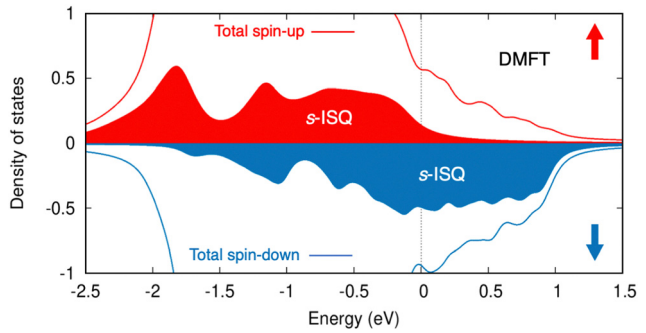

Fig. 4 Spin-resolved density of states of Li_8Au obtained by DMFT calculation at β = 30 eV^{-1}.

range (see Fig. 5 left and right panels, respectively). The half-width at half-maximum of the peak in $\langle S_z(\omega)S_z(0)\rangle$ can be used as a measure of the degree of localization.[45] The behavior of the obtained correlation functions shows that the electride states can be in two different regimes: from low temperature with β = 30 eV^{-1} (387 K) up to β = 5 eV^{-1} (2320 K) we observe extremely narrow peaks, indicating weak fluctuations and strong localization of magnetic moments. On the contrary, at the higher temperatures with β below 4 eV^{-1} the curve of the correlation function becomes flattened, signifying an itinerant regime corresponding to a paramagnetic metallic phase with weakly localized moments. The same behavior can be traced from the correlation function of imaginary time (Fig. 5 left panel). If the magnetic moments are well localized, this correlation function remains close to constant: $\langle S_z(\tau)S_z(0)\rangle \approx S^2$. This is exactly the kind of behavior we observe at $\beta \geq 5$ eV^{-1}. For $\beta \leq 4$ eV^{-1} the spin moments are delocalized, corresponding to the Fermi liquid regime. Thus, both diagrams of spin–spin correlation functions contain two distinct sets of curves with delocalized and well-localized moments corresponding to paramagnetic and ferromagnetic phases, respectively. The observed behavior of the correlation functions also suggests that the magnetic phase is stable over a wide temperature range, and the transition between the paramagnetic and ferromagnetic phases is abrupt.

Since Li_8Au has two weakly coupled conducting electron subsystems (s-ISQ and p-Au), and ISQ do not have their own

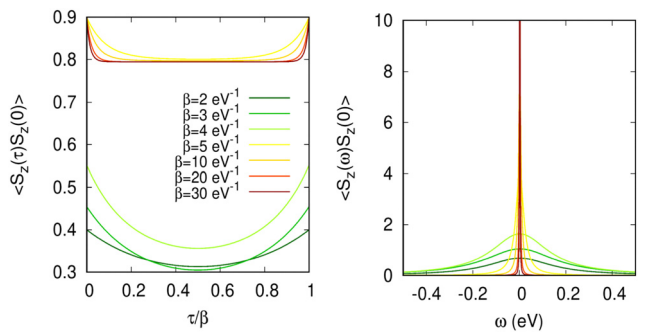

Fig. 5 Local spin–spin correlation functions on imaginary time axis (a) and on real frequencies (b).

phonon modes, the occurrence of spin polarization in the former does not necessarily exclude the possibility of realization of a superconducting state in the later,[46–50] but such a mechanism requires additional studies. If it would be confirmed that superconductivity in the p-Au subsystem is preserved despite spin ordering of interstitial electrons, Li_8Au could become a unique material where two adjacent electronic subsystems, FM-ordered and BCS-superconducting, coexist simultaneously.

3 Conclusions

In summary, our work deepens the understanding of the importance of many-body effects in the ISQ subsystem of electronic states, and reveals the mechanism of formation of IAEs intrinsic magnetic moments that behave as FM quasi-atoms. This phenomenon is realized in the Li_8Au electride, which includes strongly localized IAEs occupying specific crystallographic positions in the centers of Li_8 cubes. We calculated the value of the Coulomb parameter U for the IAE states using the CRPA method and it turned out to be comparable to the width of the partially filled ISQ energy band and equal to 2 eV, which suggests a moderate correlation regime. Using the DFT+DMFT approach, we find that well-localized magnetic moments are formed on the IAE states and spin polarization arises within the electronic subsystem of Li_8Au. Based on the assumption that the atomic (p-Au) and electride (s-ISQ) electronic subsystems are weakly coupled, the latter can be considered as a platform for studying detached electronic quantum systems with well-localized magnetic moments. In particular, this opens the way to investigate the possibility of coexistence of magnetism and superconductivity in two adjacent electronic systems. Overall, the observed many-body effects in Li_8Au indicate their importance in the study of new materials with excess electrons confined in cavities.

4 Method details

The non-interacting DFT band structure $\varepsilon(\vec{k})$ was obtained using the Quantum ESPRESSO package[51] with the exchange–correlation energy described by the generalized gradient approximation (GGA) and the Perdew–Burke–Ernzerhof (PBE) functional.[52] Structural data for Li_8Au were taken from ref. 33. Integration in the reciprocal space was performed on a regular mesh of 16 × 16 × 16 k points in the irreducible part of the Brillouin zone. The MLWF basis was obtained using the Wannier90 package,[53] which was also utilized to construct the non-interacting GGA Hamiltonian H_{GGA} in the real space. DFT+DMFT calculations were performed for the inverse temperature $\beta = 1/k_BT$ = from 2 to 30 eV^{-1}, where k_B is the Boltzmann constant and T is the absolute temperature. The effective DMFT quantum impurity problem[54] was solved using the continuous-time quantum Monte Carlo method with the hybridization expansion algorithm[55] as implemented in the package AMULET.[56]

Author contributions

D. Y. N. conceptualization, investigation and writing – original draft; D. M. K. formal analysis and writing – review & editing; A. O. S. formal analysis and writing – review & editing; V. I. A. writing – review & editing; A. R. O. writing – review & editing, project administration and funding acquisition.

Data availability

The data supporting this article have been included as part of the ESI.†

Conflicts of interest

The authors declare no conflicts of interest.

Acknowledgements

The DFT and MLWF parts of the study were supported by the Ministry of Science and Higher Education of the Russian Federation (No. 122021000039-4, theme ''Electron''). The DMFT results were obtained within the state assignment of the Russian Science Foundation (Project 19-72-30043).

References

1 S. Nie, Y. Qian, J. Gao, Z. Fang, H. Weng and Z. Wang, *Phys. Rev. B*, 2021, **103**, 205133.
2 S. Kim, J. Bang, C.-Y. Lim, S. Y. Lee, J. Hyun, G. Lee, Y. Lee, J. D. Denlinger, S. Huh, C. Kim, S. Y. Song, J. Seo, D. Thapa, S.-G. Kim, Y. H. Lee, Y. Kim and S. W. Kim, *Nat. Mater.*, 2022, **21**, 1269–1274.
3 J. Falson, I. Sodemann, B. Skinner, D. Tabrea, Y. Kozuka, A. Tsukazaki, M. Kawasaki, K. von Klitzing and J. H. Smet, *Nat. Mater.*, 2022, **21**, 311–316.
4 E. Wigner, *Phys. Rev.*, 1934, **46**, 1002–1011.
5 A. Fujimori, *Nat. Mater.*, 2022, **21**, 1217–1218.
6 H. Hosono and M. Kitano, *Chem. Rev.*, 2021, **121**, 3121–3185.
7 C. Wang, M. Xu, K. T. Butler and L. A. Burton, *Phys. Chem. Chem. Phys.*, 2022, **24**, 8854–8858.
8 H. Hosono and M. Kitano, *Chem. Rev.*, 2021, **121**, 3121–3185.
9 W. Meng, J. Wang, X. Wang, W. Wang, X. Zhang, Y. Bando and Z. Cheng, *J. Mater. Chem. A*, 2024, **12**, 2583–2604.
10 Y. Toda, S. W. Kim, K. Hayashi, M. Hirano, T. Kamiya, H. Hosono, T. Haraguchi and H. Yasuda, *Appl. Phys. Lett.*, 2005, **87**, 1–3.
11 M. Kitano, Y. Inoue, Y. Yamazaki, F. Hayashi, S. Kanbara, S. Matsuishi, T. Yokoyama, S.-W. Kim, M. Hara and H. Hosono, *Nat. Chem.*, 2012, **4**, 934–940.
12 Y. Toda, H. Hirayama, N. Kuganathan, A. Torrisi, P. V. Sushko and H. Hosono, *Nat. Commun.*, 2013, **4**, 2378.
13 J. Hu, B. Xu, S. A. Yang, S. Guan, C. Ouyang and Y. Yao, *ACS Appl. Mater. Interfaces*, 2015, **7**, 24016–24022.
14 Q. Zhu, T. Frolov and K. Choudhary, *Matter*, 2019, **1**, 1293–1303.
15 G. Wang, Y. Zhong, Y. Xu, Z. Qian, J. Jiang and Z. Ma, *Phys. Chem. Chem. Phys.*, 2023, **25**, 17300–17305.
16 D. Y. Novoselov, D. M. Korotin, A. O. Shorikov, A. R. Oganov and V. I. Anisimov, *JETP Lett.*, 2019, **109**, 387–391.
17 D. Y. Novoselov, D. M. Korotin, A. O. Shorikov, A. R. Oganov and V. I. Anisimov, *J. Phys.: Condens. Matter*, 2020, **32**, 445501.
18 D. Y. Novoselov, D. M. Korotin, A. O. Shorikov, V. I. Anisimov and A. R. Oganov, *J. Phys. Chem. C*, 2021, **125**, 15724–15729.
19 D. Y. Novoselov, V. I. Anisimov and A. R. Oganov, *Phys. Rev. B*, 2021, **103**, 235126.
20 S. Kanno, T. Tada, T. Utsumi, K. Nakamura and H. Hosono, *J. Phys. Chem. Lett.*, 2021, **12**, 12020–12025.
21 D. Y. Novoselov, M. A. Mazannikova, D. M. Korotin, A. O. Shorikov, M. A. Korotin, V. I. Anisimov and A. R. Oganov, *J. Phys. Chem. Lett.*, 2022, **13**, 7155–7160.
22 M. A. Mazannikova, D. M. Korotin, V. I. Anisimov, A. R. Oganov and D. Y. Novoselov, *JETP Lett.*, 2023, **118**, 664–670.
23 M. A. Mazannikova, D. M. Korotin, A. O. Shorikov, V. I. Anisimov and D. Y. Novoselov, *J. Phys. Chem. C*, 2023, **127**, 8714–8719.
24 D. Y. Novoselov, M. A. Mazannikova, D. M. Korotin, A. O. Shorikov, V. I. Anisimov and A. R. Oganov, *Phys. Chem. Chem. Phys.*, 2023, **25**, 30960–30965.
25 J. Park, K. Lee, S. Y. Lee, C. N. Nandadasa, S. Kim, K. H. Lee, Y. H. Lee, H. Hosono, S.-G. Kim and S. W. Kim, *J. Am. Chem. Soc.*, 2017, **139**, 615–618.
26 J. Zhou, Y. P. Feng and L. Shen, *Phys. Rev. B*, 2020, **102**, 180407.
27 S. Liu, C. Wang, H. Jeon, Y. Jia and J.-H. Cho, *Phys. Rev. B*, 2022, **105**, L220401.
28 S. Y. Lee, J.-Y. Hwang, J. Park, C. N. Nandadasa, Y. Kim, J. Bang, K. Lee, K. H. Lee, Y. Zhang, Y. Ma, H. Hosono, Y. H. Lee, S.-G. Kim and S. W. Kim, *Nat. Commun.*, 2020, **11**, 1526.
29 J.-F. Zhang, D. Xu, X.-L. Qiu, N.-N. Zhao, Z.-Y. Lu and K. Liu, *J. Phys. Chem. C*, 2023, **127**, 696–701.
30 H. Y. Song, B. I. Yoo, J.-H. Choi, S.-H. Kang, J. Bang, W. Li, C. N. Nandadasa, D. Thapa, D. Yoon, M. J. Han, K. H. Lee, S. G. Kim, K. Lee and S. W. Kim, *Mater. Today Phys.*, 2021, **20**, 100473.
31 S. Y. Lee, D. C. Lim, M. S. Khan, J. Y. Hwang, H. S. Kim, K. H. Lee and S. W. Kim, *Nat. Commun.*, 2023, **14**, 5469.
32 X. Zhang, W. Meng, Y. Liu, X. Dai, G. Liu and L. Kou, *J. Am. Chem. Soc.*, 2023, **145**, 5523–5535.
33 X. Zhang, Y. Yao, S. Ding, A. Bergara, F. Li, Y. Liu, X.-F. Zhou and G. Yang, *Phys. Rev. B*, 2023, **107**, L100501.
34 I. A. Troyan, D. V. Semenok, A. G. Ivanova, A. G. Kvashnin, D. Zhou, A. V. Sadakov, O. A. Sobolevsky, V. M. Pudalov, I. S. Lyubutin and A. R. Oganov, *Phys.-Usp.*, 2022, **65**, 748–761.
35 X. Dong, A. R. Oganov, A. F. Goncharov, E. Stavrou, S. Lobanov, G. Saleh, G.-R. Qian, Q. Zhu, C. Gatti, V. L. Deringer, R. Dronskowski, X.-F. Zhou, V. B. Prakapenka, Z. Konôpková,

I. A. Popov, A. I. Boldyrev and H.-T. Wang, *Nat. Chem.*, 2017, **9**, 440–445.
36 M. S. Miao and R. Hoffmann, *Acc. Chem. Res.*, 2014, **47**, 1311–1317.
37 A. D. Becke and K. E. Edgecombe, *J. Chem. Phys.*, 1990, **92**, 5397–5403.
38 N. Marzari, A. A. Mostofi, J. R. Yates, I. Souza and D. Vanderbilt, *Rev. Mod. Phys.*, 2012, **84**, 1419–1475.
39 G. Vasseur, Y. Fagot-Revurat, B. Kierren, M. Sicot and D. Malterre, *Symmetry*, 2013, **5**, 344–354.
40 M. Springer and F. Aryasetiawan, *Phys. Rev. B: Condens. Matter Mater. Phys.*, 1998, **57**, 4364–4368.
41 T. Kotani, *J. Phys.: Condens. Matter*, 2000, **12**, 2413–2422.
42 A. Georges, G. Kotliar, W. Krauth and M. J. Rozenberg, *Rev. Mod. Phys.*, 1996, **68**, 13–125.
43 H. J. Vidberg and J. W. Serene, *J. Low Temp. Phys.*, 1977, **29**, 179–192.
44 J. Heyd, G. E. Scuseria and M. Ernzerhof, *J. Chem. Phys.*, 2003, **118**, 8207–8215.
45 A. A. Katanin, A. I. Poteryaev, A. V. Efremov, A. O. Shorikov, S. L. Skornyakov, M. A. Korotin and V. I. Anisimov, *Phys. Rev. B: Condens. Matter Mater. Phys.*, 2010, **81**, 045117.
46 N. I. Karchev, K. B. Blagoev, K. S. Bedell and P. B. Littlewood, *Phys. Rev. Lett.*, 2001, **86**, 846–849.
47 A. O. Shorikov, V. I. Anisimov and M. Sigrist, *J. Phys.: Condens. Matter*, 2006, **18**, 5973–5983.
48 S. S. Saxena, P. Agarwal, K. Ahilan, F. M. Grosche, R. K. W. Haselwimmer, M. J. Steiner, E. Pugh, I. R. Walker, S. R. Julian, P. Monthoux, G. G. Lonzarich, A. Huxley, I. Sheikin, D. Braithwaite and J. Flouquet, *Nature*, 2000, **406**, 587–592.
49 J. Wang, M. Singh, M. Tian, N. Kumar, B. Liu, C. Shi, J. K. Jain, N. Samarth, T. E. Mallouk and M. H. W. Chan, *Nat. Phys.*, 2010, **6**, 389–394.
50 A. B. Karki, V. O. Garlea, R. Custelcean, S. Stadler, E. W. Plummer and R. Jin, *Proc. Natl. Acad. Sci. U. S. A.*, 2013, **110**, 9283–9288.
51 P. Giannozzi, S. Baroni, N. Bonini, M. Calandra, R. Car, C. Cavazzoni, D. Ceresoli, G. L. Chiarotti, M. Cococcioni, I. Dabo, A. Dal Corso, S. de Gironcoli, S. Fabris, G. Fratesi, R. Gebauer, U. Gerstmann, C. Gougoussis, A. Kokalj, M. Lazzeri, L. Martin-Samos, N. Marzari, F. Mauri, R. Mazzarello, S. Paolini, A. Pasquarello, L. Paulatto, C. Sbraccia, S. Scandolo, G. Sclauzero, A. P. Seitsonen, A. Smogunov, P. Umari and R. M. Wentzcovitch, *J. Phys.: Condens. Matter*, 2009, **21**, 395502.
52 J. P. Perdew, K. Burke and M. Ernzerhof, *Phys. Rev. Lett.*, 1996, **77**, 3865–3868.
53 A. A. Mostofi, J. R. Yates, G. Pizzi, Y.-S. Lee, I. Souza, D. Vanderbilt and N. Marzari, *Comput. Phys. Commun.*, 2014, **185**, 2309–2310.
54 P. Werner and A. J. Millis, *Phys. Rev. B: Condens. Matter Mater. Phys.*, 2006, **74**, 155107.
55 E. Gull, A. J. Millis, A. I. Lichtenstein, A. N. Rubtsov, M. Troyer and P. Werner, *Rev. Mod. Phys.*, 2011, **83**, 349–404.
56 **https://www.amulet-code.org**.